Received: 14 June 2018 | Revised: 11 July 2019 | Accepted: 22 July 2019

DOI: 10.1002/nbm.4186

RESEARCH ARTICLE

WILEY NMR IN BIOMEDICINE

Multiparametric classification of sub-acute ischemic stroke recovery with ultrafast diffusion, ^{23}Na, and MPIO-labeled stem cell MRI at 21.1 T

Avigdor Leftin[1,4] | Jens T. Rosenberg[2] | Xuegang Yuan[3] | Teng Ma[3] | Samuel C. Grant[2,3] | Lucio Frydman[1,3]

[1] Department of Chemical and Biological Physics, Weizmann Institute of Science, Rehovot, Israel

[2] The National High Magnetic Field Laboratory, Florida State University, Tallahassee, FL, USA

[3] FAMU-FSU Chemical and Biochemical Engineering, Florida State University, Tallahassee, FL, USA

[4] Department of Radiology, Stony Brook Medicine, Stony Brook University, Stony Brook, NY, USA

Correspondence
Avigdor Leftin, Department of Radiology, Stony Brook Medicine, Stony Brook University, Stony Brook, NY, USA.
Email: avigdor.leftin@stonybrookmedicine.edu

Funding information
American Heart Association, Grant/Award Number: 10DRNT3860040; Fulbright Association; Minerva Foundation, Grant/Award Number: 712277; National Science Foundation, Grant/Award Numbers: 1064075, DMR-1157490 and DMR-1644779; National Institutes of Health, Grant/Award Number: R01 NS102395

MRI leverages multiple modes of contrast to characterize stroke. High-magnetic-field systems enhance the performance of these MRI measurements. Previously, we have demonstrated that individually sodium and stem cell tracking metrics are enhanced at ultrahigh field in a rat model of stroke, and we have developed robust single-scan diffusion-weighted imaging approaches that utilize spatiotemporal encoding (SPEN) of the apparent diffusion coefficient (ADC) for these challenging field strengths. Here, we performed a multiparametric study of middle cerebral artery occlusion (MCAO) biomarker evolution focusing on comparison of these MRI biomarkers for stroke assessment during sub-acute recovery in rat MCAO models at 21.1 T. T_2-weighted MRI was used as the benchmark for identification of the ischemic lesion over the course of the study. The number of MPIO-induced voids measured by gradient-recalled echo, the SPEN measurement of ADC, and ^{23}Na MRI values were determined in the ischemic area and contralateral hemisphere, and relative performances for stroke classification were compared by receiver operator characteristic analysis. These measurements were associated with unique time-dependent trajectories during stroke recovery that changed the sensitivity and specificity for stroke monitoring during its evolution. Advantages and limitations of these contrasts, and the use of ultrahigh field for multiparametric stroke assessment, are discussed.

KEYWORDS

diffusion, MRI, multiparametric, sodium, stem cell tracking, stroke, ultrahigh field

Abbreviations: ADC, apparent diffusion coefficient; AUC, area under the curve; DW, diffusion weighted; FOV, field of view; GRE, gradient recalled echo; hMSC, human mesenchymal stem cell; IA, intra-arterial; MCAO, middle cerebral artery occlusion; MPIO, micrometer-sized particle of iron oxide; RARE, rapid acquisition with relaxation enhancement; ROC, receiver operator characteristic; ROI, region of interest; SPEN, spatiotemporal encoding.

Avigdor Leftin and Jens T. Rosenberg Contributed equally to this study.
Samuel C. Grant and Lucio Frydman Co-senior authorship.

1 | INTRODUCTION

Ischemic stroke remains one of the leading causes of neurological problems and death, but imaging methods such as CT, MRI, and others together with new therapies have succeeded in reducing complications and morbidity following occlusion.[1-3] Out of these, MRI has become a benchmark in stroke imaging because it enables early detection, as well as longitudinal measurements for monitoring stroke progression and response to treatment.[4] Established MRI measurements of stroke leverage combinations of T_2-weighted MRI, perfusion imaging, and diffusion-weighted (DW) imaging, and most recently sodium MRI to report on vascular interruption and edema, swelling in brain microstructures, and perturbation of electrolyte balance, respectively.[4-8] During the sub-acute recovery phase, MRI also can be used to track homing of cellular theranostics such as stem cells using iron nanoparticles as an indicator of delivery in re-perfused tissue regions.[9,10]

Increased magnetic field can enhance MRI contrasts, motivating a push towards higher field in both preclinical and clinical MRI scanners that improve MRI measurements to better characterize cerebral ischemia in animal models and humans.[11] The main advantage of using high-field MRI is increased signal-to-noise ratio (SNR). An approximate B_0 magnetic field strength scaling for protons of SNR $\propto B_0^{1.65}$ is observed, which tapers off to a more linear increase between 9.4 and 21.1 T. For X nuclei such as ^{23}Na, conducting these scans at the highest small animal imaging system to date, 21.1 T provides up to a threefold gain in sensitivity compared with preclinical tests previously conducted at 9.4 T.[12,13] Higher SNR provides higher-contrast images for stroke detection with reduced scan times,[13-15] and improved quantification of apparent diffusion coefficient (ADC) utilizing high b-values.[16] Enhancement of local susceptibility contrast needed for detection of paramagnetic-labeled cells in the brains of ischemic animals is also maximized for iron nanoparticles.[17-19]

While the anatomical, microstructural, cellular, and molecular information obtainable from different MRI methods is enhanced at high magnetic field, ultimately the power of each these measurements to detect and monitor stroke depends on the sensitivity and specificity of each parameter and its changes during stroke recovery.[20-22] To characterize the evolution of these parameters and their utility for classification at ultrahigh field, a middle cerebral artery occlusion (MCAO) model of ischemic stroke in rats was studied using a multiparametric MRI approach at 21.1 T. Sub-acute ischemic recovery was followed using T_2-weighted stroke measurements, ultrafast spatiotemporal encoded (SPEN) diffusion imaging of ADC, human mesenchymal stem cell (hMSC) tracking with high-susceptibility micrometer-sized particles of iron oxide (MPIOs), and sodium (^{23}Na) MRI. The various indicators of stroke derived from these image contrasts were evaluated and tested according to their ability to serve as biomarkers of stroke recovery, and their performance evaluated in terms of sensitivity and specificity for stroke classification in the receiver operator characteristic (ROC) sense. These high-field trials indicate that these individual measurements vary in their trajectories during recovery, affecting their ability to classify tissue according to their different sensitivities and specificities for the multiparametric aspects of stroke.

2 | METHODS

2.1 | MCAO and transplantation of MPIO-labeled cells

The Florida State University Animal Care and Use Committee approved all animal use and surgical procedures. MCAO was performed following surgical procedures previously reported.[16] For MRI cell tracking, 0.86 μm diameter MPIOs (Bangs Laboratories, Fishers, IN, USA) were used to label bone-marrow-derived hMSCs obtained from the Tulane Center for Gene Therapy (Tulane University, New Orleans, LA, USA). Cells were labeled overnight by adding sterile particles to a monolayer cell culture as previously reported.[17] Prior to in vivo injection, hMSCs were subjected to short-duration, sub-lethal hypoxic preconditioning (0.5% O_2 for 24 h) to increase their viability and initial homing to the ischemic lesion.[23] Intra-arterial (IA) injections of the contrast-labeled hMSCs were performed immediately after the MCAO in each animal using the exposed carotid artery. The IA injection technique provides a direct route to the brain while also promoting single-cell delivery.

2.2 | MRI

Experiments were carried out on the ultrawide-bore 21.1 T (900 MHz) vertical magnet built at the National High Magnetic Field Laboratory in Tallahassee, FL, USA.[24] The magnet is equipped with a Bruker Avance III console, ParaVision 5.1 and 6.0.1 acquisition and processing software (Bruker BioSpin, Billerica, MA, USA), and 64 mm inner diameter imaging gradients (Resonance Research, Billerica, MA, USA) capable of producing 0.6 T/m peak gradient strengths. For ^{1}H imaging, a 33 mm homebuilt quadrature surface coil was used with the animal suspended with a bite bar and hook-and-loop straps (Velcro, AZ, USA).[25] For ^{23}Na imaging, a ^{1}H/^{23}Na birdcage volume resonator was used with the same animal restraint and positioning.[13] During the MRI experiments (<1 h each session), oxygen mixed with 2–3% isoflurane was continuously provided through the bite bar and respiration rate was monitored using a pneumatic pillow (SA Instruments, Stony Brook, NY, USA). The animal was kept at a constant 37°C body temperature.

The following MRI experiments were conducted in the same imaging session on all animals 1, 3, and 7 d after MCAO and hMSC injection: (1) ^{1}H 2D T_2-weighted rapid acquisition with relaxation enhancement (RARE) scans acquired with an acceleration factor of 4 and 300 phase encodes,

$T_R/T_E/T_{Eeff}$ = 6 s/13 ms/26 ms, two averages, 15 min 0 s total scan time, a field of view (FOV) of 25.6 × 30 mm^2, and resolution of 0.10 × 0.10 × 0.5 mm^3 for stroke lesion measurement; (2) ^{1}H 2D gradient recalled echo (GRE) sequence with T_R/T_E = 725/5 ms, two averages, 12 min 22 s total scan time, 70° flip angle, FOV = 25.6 × 25.6 and resolution 0.05 × 0.05 × 0.3 mm^3 for cell tracking; (3) single-slice, single-scan ^{1}H 2D DW-SPEN images, T_R = 12 s and effective T_E = 40 ms, which is determined by the frequency-swept chirp pulse duration (sweep width 10 kHz, effective bandwidth 250 kHz), FOV = 32 × 32 mm^2 and an in-plane resolution of 0.32 × 0.32 × 2 mm^3 for ADC mapping (six nominal *b*-values were used, 0, 200, 400, 600, 800, and 1000 s/mm^2, applied separately along the *x*, *y*, and *z* directions with = 9.81 and 3.5 ms with 3 min 36 s total scan time). (4) Cartesian-sampled 3D ^{23}Na GRE acquisitions were performed on these same animals at 2, 4, and 8 d after MCAO and hMSC injection, T_E/T_R = 1/50 ms, 36 averages, 30 min 43 s total scan time, FOV = 32 × 32 × 32 mm^3, and a matrix size of 32 × 32 × 32 resulting in 1 mm isotropic resolution for mapping sodium levels.

2.3 | MRI data processing

Image reconstruction was performed for ^{1}H RARE, ^{1}H GRE, and 3D ^{23}Na MRI data using Bruker ParaVision and ImageJ. ^{1}H SPEN images were processed, reconstructed using a super-resolution algorithm,[26] and analyzed with a combination of ParaVision, MATLAB (MathWorks, Natick, MA, USA), and ImageJ. DW-SPEN ADC maps were calculated using a pixel-by-pixel fit with a two-parameter exponential decay function, and background gradient correction performed as previously described.[27] Stroke lesion was identified on T_2-weighted imaging. Accordingly, the mid-section of the stroke volume was identified and the DW-SPEN slice was acquired in this position. RARE, GRE, and ^{23}Na images were resliced and resized to generate axial images and aligned according to anatomical landmarks with single SPEN slices referencing the midsection of the stroke. Reproducible animal positioning was not an issue due to the design of the RF probe animal bed. RARE images were used to define a stroke region of interest (ROI) drawn manually, which was then used for analysis of all other measurements. Control measurements corresponded to a contralateral ROI. Mean ADC values were determined from these ROIs in DW-SPEN ADC maps. GRE images were background corrected, and thresholded to identify hypointense voids corresponding to MPIO-labeled hMSCs that were detected and counted within the ROI using the ImageJ Analyze Cluster tool summing three image slices within the midpoint stroke region. Mean ^{23}Na intensity was measured in ischemic and ipsilateral areas using ROI tools.

2.4 | Statistics

The study uses the longitudinal imaging data from stroked rats (n = 5) exhibiting MRI-confirmed MCAO stroke and MPIO-labeled hMSC IA delivery to the ischemic lesion 1 d after MCAO. The retrospective design of the study addresses (1) evolution of biomarker contrast for stroke using mean integrated contralateral (control) and ipsilateral (ischemia) MRI measurements made at the various study time points, and (2) ROCs of the MRI measurements at each time point and cumulatively for all time points. ^{1}H RARE T_2-weighted MRI measurements were used to define the binary response variable for the ROC classifier of stroke by which the performance of the other MRI measurements was evaluated. The positive presence of stroke was indicated by ischemia in the ipsilateral hemisphere of the T_2-weighted images, and regions of interest were drawn manually around this area by tracing the high-contrast interface between the ischemic stroked and unaffected tissue and translated to the contralateral hemisphere as the negative response variable. The multi-parametric assessments of stroke were evaluated in these regions and used as predictor variables for the classification of the presence or absence of stroke. These models were fit according to a logistic regression (fitglm), followed by construction of ROC curves of the true positive (sensitivity) versus false positive rate (1 − specificity) by using the probability estimates of the regression model as input scores (perfcurve), and calculating the normalized area under the curve (AUC) values as metrics of the single and combination MRI measurements for stroke detection in MATLAB. This analysis was performed at each time point, and repeated in a cumulative analysis for all time points. All other statistical tests were calculated with GraphPad Prism 7 (GraphPad Software, San Diego, CA, USA) using $p < 0.05$ as the significance cutoff.

3 | RESULTS

3.1 | MRI of sub-acute ischemic recovery at 21.1 T

Figure 1 shows representative MR images from the study. Figure 1A shows ^{1}H RARE T_2-weighted images that evidence ischemic lesions generated by the MCAO found localized in the striatum. Areas of elevated T_2-weighted contrast were largest at the initial study time point and decreased over the study duration, but were still observable even at late time points indicating partial stroke edema recovery. hMSC delivery was confirmed by the appearance of punctate hypointense voids detected primarily in the penumbral regions of the stroke lesion in all animals at initial time points, and remained present at all time points according to ^{1}H GRE images in Figure 1B. ^{23}Na images detected stroke according to elevated sodium in striatal regions compared with the contralateral brain regions, and volumes of ^{23}Na signal appeared to shrink in a similar

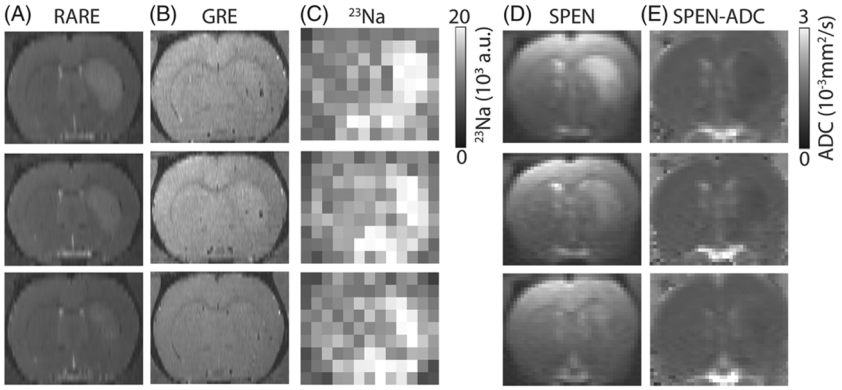

FIGURE 1 In vivo MRI measurements of rat MCAO stroke model at 21.1 T. representative ^{1}H RARE T_2-weighted (a), ^{1}H GRE T_1-weighted (B), ^{23}Na 3D GRE (C), and ^{1}H SPEN T_2-weighted (b_0) (D) images and ^{1}H SPEN-ADC maps (E) at longitudinal study time-points (1, 3, and 7 d (a, B, D, E) and 2, 4, and 8 d (C) after MCAO in top to bottom rows)

manner to the T_2-weighted benchmarks while signal intensity remained elevated over time. Single-scan b = 0 DW-SPEN images in Figure 1D showed regions of stroke according to elevations in T_2-weighted contrast, and SPEN-ADC maps revealed reduced ADC in the lesion and a corresponding pseudonormalization of ADC level during recovery.

3.2 | Quantification of stroke biomarker evolution and ROC performance

Figure 2A shows the behavior of the number of MPIO-induced voids in the ischemic ipsilateral and contralateral control ROIs over time. MPIO void counts indicated that the majority of animals showed a reduction of the number of voids in the ipsilateral regions over time, though two animals exhibit a small trend towards more voids over time, suggestive of infarct or microhemorrhage. A small unexplained transient increase in voids in the contralateral region was also observed at the second time point, but this recovered to baseline at the endpoint. Overall, there were no statistically significant changes in MPIO voids detected with respect to the first imaging time point in either the ipsilateral or contralateral regions for either of the measurements. The ROC analyses of MPIO-void measurements are shown in Figure 2B-D for each of the time points, and in Figure 2 E for the cumulative set of measurements. Integrated areas of the contralateral and ipsilateral void measurements were used as input predictor variables, and T_2-weighted MRI as the response variable of the analysis. Thus, the ROC curves indicate relative performance for stroke classification according to the ability to separate stroke versus healthy tissue defined by T_2-weighted imaging by integrated ROI measurements of number of MPIO, or other, voids. As no significant differences in longitudinal measurements of voids were observed between the time points, and there is

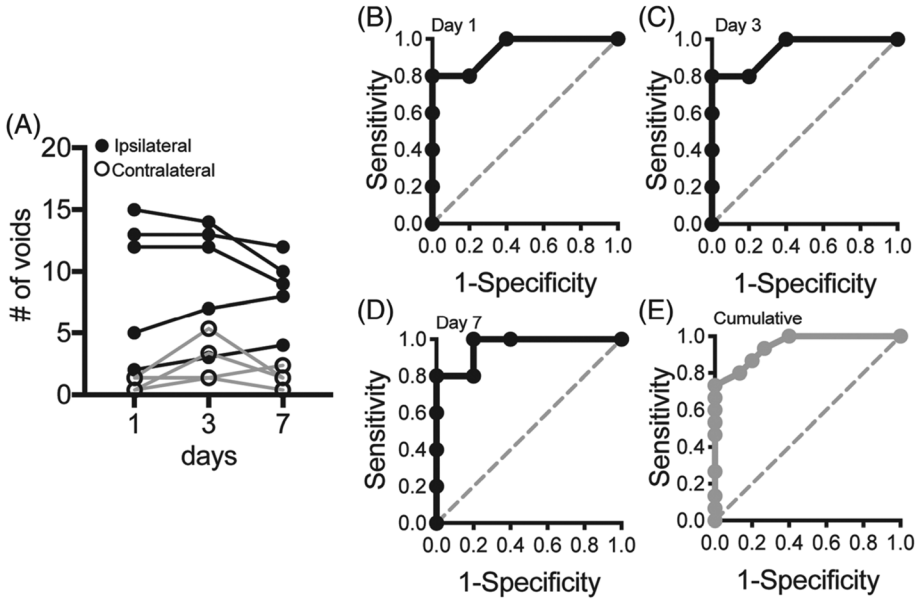

FIGURE 2 Stroke biomarker evolution and ROC analysis of MPIO-hMSCs. A, number (#) of MPIO-labeled hMSC voids in ipsilateral (ischemic) and contralateral ROI (control) as a function of days after MCAO. Analysis done with n = 5 rats, two-way ANOVA with Tukey's multiple comparison tests. Not significant. B-D, ROC curve of sensitivity versus 1 − specificity of MPIO-hMSC voids on day 1, day 3, and day 7; E, cumulative ROC curve for all timepoints

some overlap between contralateral and ipsilateral measurements of voids in the ROI analysis, it is expected that the ROC performance of the curves remains similar over time points and exhibits lower sensitivity for stroke classification compared with specificity, as the ipsilateral regions consistently exhibited more voids than did the contralateral between subjects. Indeed, normalized AUC measurements remained high for MPIO voids at the three measurement time points (0.94, 0.94, 0.96), and false positive (1 − specificity) values (0, 0, 0) were low compared with true positive (sensitivity) values (0.8, 0.8, 0.8) given by the optimum operating point metric of the ROC analysis. Cumulative analysis of the combined time points confirmed that overall AUC performance and false positive values remained good at 0.94 and 0 respectively, while MPIO voids used as predictor variables of stroke suffer from low sensitivity values overall at 0.73.

Figure 3A shows the ^{1}H SPEN-ADCs plotted over time for ipsilateral and contralateral ROIs at the three time points measured. Longitudinal trajectories of the ipsilateral and contralateral measurements recapitulate the known pseudonormalization behavior of rodent ADC during stroke recovery, for which significant recovery of lower ADC values towards higher normal brain ADC is observed in the second ($p < 0.05$) and last ($p < 0.01$) imaging time point with respect to the first. Early time points of the ADC measurements were distinctly separated from the contralateral reference, and ROC analysis of Day 1 (Figure 3B) and Day 3 (Figure 3C) measurements reflect this aspect, as AUC = 1 values for each of these measurement sets indicate that the ADC functions as a perfect classifier of stroke with respect to the T_2-weighted MRI response variable benchmark. Correspondingly, optimal operating points of these ROC curves gave false positive rates of 0 and true positive rates of 1. However, on Day 7 after MCAO the ROC performance curves of ADC were distinctly different from earlier measurements, reflecting the pseudonormalization of the ADC. Figure 3D shows that on Day 7 the ROC AUC for ADC falls to 0.84, due to the decrease in sensitivity to 0.6, while the false positive (1 − specificity) value remained at 0. Thus, the overall ROC performance of the ADC shown in Figure 3E remained high at 0.95; lower sensitivity at 0.86 occurs due to changes in ADC value over time, although ADC specificity remained high.

Integrated ROI of ipsilateral and contralateral ^{23}Na MRI were also compared and shown over time in Figure 4A. ^{23}Na MRI measurements of stroke exhibit a trend to lower values over time, reaching significance ($p < 0.05$) by the last time point, while contralateral levels remain constant. However, sodium levels remain elevated over the course of the study, indicating that they likely serve as long-term predictors of stoke with respect to T_2-weighted response benchmarks. Figure 4B-4E shows the ROC curves for the ^{23}MRI measurements, confirming this observation. At each time point measured in this study the ROC AUC indicated that ^{23}Na served as a perfect classifier of stroke, as AUC = 1 and true positive and false positive rates were 1 and 0 respectively. This indicates that ^{23}Na MRI has high sensitivity and specificity for stroke at both early and later time points during sub-acute recovery, and cumulatively confirming that longitudinal trends in ^{23}Na measurements do not affect the performance of this biomarker for stroke classification.

4 | DISCUSSION

This study presents a series of MRI assessments of ischemia and its recovery at ultrahigh field for an in vivo rat MCAO model, seeking in particular to determine the relative performance of these biomarkers for stroke classification in the ROC sense compared with T_2-weighted MRI

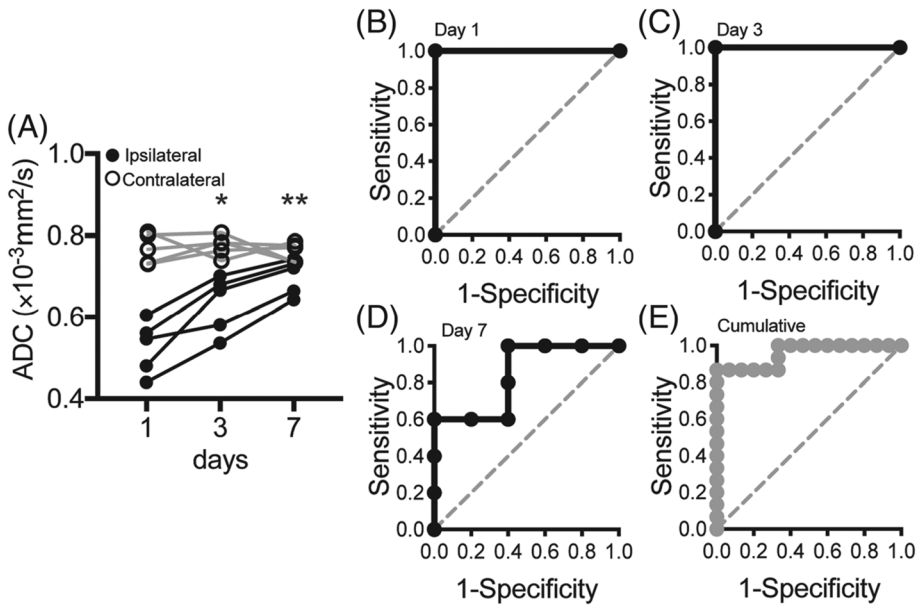

FIGURE 3 Stroke biomarker evolution and ROC analysis of DW-SPEN ADC. A, ADC in ipsilateral (ischemic) and contralateral ROI (control) as a function of days after MCAO. Analysis done with $n = 5$ rats, two-way ANOVA with Tukey's multiple comparison tests, $^{*}p < 0.05$, $^{**}p < 0.01$. B-D, ROC curve of sensitivity versus 1 − specificity of ADC on day 1, day 3, and day 7; E, cumulative ROC curve for all timepoints

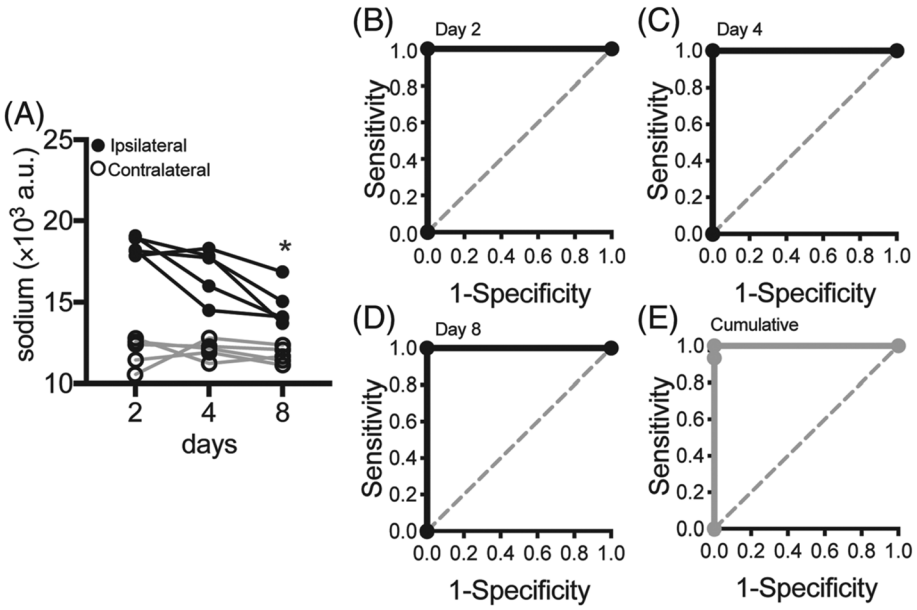

FIGURE 4 Stroke biomarker evolution and ROC analysis of ^{23}Na MRI. A, ^{23}Na in ipsilateral (ischemic) and contralateral ROI (control) as a function of days after MCAO. Analysis done with $n = 5$ rats, two-way ANOVA with Tukey's multiple comparison tests, $^{*}p < 0.05$. B-D, ROC curve of sensitivity versus 1 − specificity of ^{23}Na on day 2, day 4, and day 8; E, cumulative ROC curve for all time points

benchmarks. Results show that each MRI measurement exhibits unique longitudinal behavior, affecting its differential ability to classify stroke in its sub-acute recovery phase. Here, the significance and limitations of the study observations are presented, and advantages and challenges of performing these measurements at high field are discussed.

4.1 | Significance of ischemic measurements in the sub-acute recovery phase at high magnetic field

In this study, we utilized an ROI based on the ^{1}H RARE T_2-weighted images as an anatomical reference measurement for delineation of the ischemic stroke boundary, though identification of the lesion margins has been done in previous studies using ADC or ^{23}Na contrasts.[7,8] ADC and sodium are known to be markers associated with infarct core.[28-30] In the SPEN scans, ischemia could be detected readily utilizing the T_2-weighted bright contrast imparted by the 40 ms effective echo time, and by the reduced ADC values of the quantitative diffusion maps. Similarly, elevations of ^{23}Na in the ipsilateral hemisphere indicated the presence of stroke over the course of the study. MPIO voids were mostly found at the edges of lesions, suggesting that they served as markers of hMSC perfusion to the penumbral areas, which is supported by earlier MPIO studies that have shown them to localize in vascularized, perfused regions in the brain.[10,19,31-33] Although MPIO detection was significantly associated with MCAO rather than contralateral striatal regions, ^{1}H T_1-weighted GRE hypointense contrast did not fully demarcate the stroke borders, and thus would not serve as an optimal anatomical reference for these time courses. Thus, these observations indicate differences in the ability of the MRI biomarkers to characterize stroke and recovery.

The ROC analysis of the imaging biomarkers confirmed differences in their performance for stoke classification during this recovery phase. The classification of stroke in the analysis was related to parameter evolution. Classification of stroke depends on the degree of separation of quantified MRI measurements of the stroke and contralateral ROIs, made with respect to T_2-weighted MRI used as the response variable benchmark. Given that the cohort of animals was selected according to ischemic presence and homogeneity, the AUCs of the sensitivity and specificity ROC curves indicate their performance relative to T_2-weighted MRI alone, rather than the ability to determine stroke borders such as penumbra versus core, or for a priori stroke detection with respect to another benchmark such as pathology.[20,21,34,35] MPIO-labeled hMSCs are intended to provide a metric of initial re-perfusion of the ischemic lesion immediately after MCAO, and long-term engraftment of stem cells used for cellular therapy. Therefore, as perfusion can vary from animal to animal, the percentage of ROIs containing voids differed within the cohort, and the voids also could reflect vasculature hemorrhage, or cellular debris that can be resolved with penumbral recovery, and therefore are not strictly associated with long-term MPIO retention or hMSC engraftment. As hMSCs home to penumbral regions of the stroke, which according to T_2-weighted contrast are intermediate between normal and edema regions, AUC values for classifying stroke or not-stroke according to this parameter were the lowest, but still excellent, with AUC > 0.9, similar to the ADC and sodium AUC metrics. ADC was by far the most responsive to ischemic recovery according to its pseudonormalization over time reflecting recovery of edema and swelling, as has been shown previously in small animal models.[22,36] Cumulatively, ADC outperformed MPIO-based classification of stroke, but longitudinal analysis of ADC ROC AUC showed that,

because ADC exhibits pseudorecovery at late time points, this parameter suffers performance losses for stroke classification compared with MPIO tracking and sodium level. Sodium signal remained elevated compared with contralateral regions, similar to T_2-weighted measurements, in accord with what has been previously reported,[30,37] and its persistent elevation indicates that ^{23}Na level is a biomarker associated with change in cellular function that is compromised over longer durations than this study.[38] ^{23}Na imaging performed best over the study, as integrated ipsilateral and contralateral measurements remained well separated and were not subject to the same extent of normalization as the ADC, thus providing the best performance for stroke classification according to high sensitivity and specificity values with respect to T_2-weighted imaging. Therefore, each MRI parameter exhibits different performance for stroke classification according to its unique time and spatial dependence on stroke evolution.

4.2 | Advantages and challenges of high-field stroke imaging

High-field MRI presents a number of advantages as well as challenges for stroke imaging. While high-field systems provide increased SNR that can offer higher contrast per unit scan time, they also introduce field-dependent effects on relaxation times and susceptibility. These factors can be exploited given appropriate protocols, or can offset some of the high-field gains if not properly compensated. The current measurements highlight these tradeoffs. High resolution ^{1}H RARE T_2-weighted and GRE T_1-weighted MRI acquisitions were performed with only two averages, and ADC maps were acquired with one average per *b*-value. Assuming only a linear B_0 dependence on SNR and similar scan durations, imaging at 9.4 T would require more than four times the number of scans, and at 3 T more than 50 times the averages would be required to achieve equivalent SNR gains over reported measurements.[5,39] However, increasing T_1 relaxation times at high field and generally lower T_2 relaxation times complicate this simple estimation, though more importantly these factors contribute substantially to enhanced contrast for ^{1}H. By utilizing RARE fast multi-spin echo sequences, the rat brain could be sampled efficiently while keeping repetition times short and effective T_E long to provide high contrast for edema. For GRE acquisitions, we capitalize on added T_1 sensitivity, higher susceptibility contrast, and SNR to achieve higher spatial resolution with increased sensitivity to the MPIO label. Similarly, we exploit the higher SNR to acquire multiple-*b*-value DW images with single averages, and utilize SPEN with quadratic phase encoding, which is robust against susceptibility artifacts introduced by low-bandwidth, linear phase encoding common to conventional EPI approaches. For X nuclei such as ^{23}Na, these gains are even more significant, with comparable SNR achieved with 36 averages at 21.1 T requiring approximately 100 averages at 9.4 T and more than 300 averages at 3 T if similar ^{23}Na MRI acquisition protocols are utilized.[8,30,38,40]

4.3 | Limitations of the study

This study presents a number of MRI stroke measurements to validate and compare their performance and set a precedent for utilizing high field for future preclinical and clinical stroke imaging investigations. However, the current study and the measurements selected contain certain limitations. First, in terms of overall study design, we selected a set of MCAO animals to analyze, which were curated in terms of lesion uniformity: all animals had stroke lesions within a given size range and in the same location, and each was confirmed to contain MPIO in the initial imaging session. The cohort therefore lacks the usual heterogeneity encountered in clinical stroke research, and as such longitudinal trends and ROC performance of the measurements will likely differ from real-world applications for which the duration of occlusion and regional heterogeneity plays a major role in dictating parameter performance.[4,41-43] Further, no control group was included to evaluate the overall therapeutic effects of hMSCs. Rather, we include measurement of MPIO-labeled hMSCs as an additional parameter sensitive mostly to re-perfusion that exhibits high contrast at ultrahigh magnetic field. To fully address therapeutic potential of the hMSCs, additional cohorts, cell-culture manipulations, longitudinal histopathology, and functional assays are required[9,10,36,44] and underway at 21.1 T. Thus, these measurements serve as a baseline for validating the multiparametric measurements, including an hMSC tracking approach for future theranostic investigations.

This study included MPIO-labeled hMSC tracking, ADC measurements, and ^{23}Na imaging, measurements of ongoing interest due to efforts in advancing high-field stroke research, as well as in the context of theranostic interventions.[13,15-19,24,45-47] Our focus on these imaging approaches and characterization of sub-acute timelines differ somewhat from previous combinations of perfusion and diffusion imaging during acute stroke onset.[4,22,29,35,37,39,44] Our approaches differ in that they evaluate their longitudinal performance for ischemic detection at later time points using ROCs in confirmed cases rather than using this statistic to generate predictive models of the recovery, or focus on regional interpretation of stroke heterogeneity based on penumbra versus core distribution,[1,29,30,34,42] though these evaluations are extremely important. Therefore our study is mainly focused in validating these biomarkers at 21.1 T to support further applications and integration of these methods with conventional approaches that have established their utility as diagnostic or prognostic metrics in preclinical and clinical settings.

4.4 | Outlook and conclusions

To continue the development of these applications a number of technical improvements that can better address the needs of the stroke research community are desirable. First, despite the 21.1 T magnet system providing the highest SNR, noise trade-offs with scan duration and image

resolution are still a major concern. This gap is especially large when comparing high-resolution fast ^{1}H GRE-based MPIO tracking and relatively slow and low-resolution ^{23}Na acquisitions. While previous studies have been conducted using these mismatched resolutions, this issue remains a significant constraint on identifying pixel-wise multiparametric correspondence and establishing direct regional correlations. These improvements potentially can be achieved by utilizing ultrashort echo acquisitions that better sample the fast decay (T_2) of the quadrupolar ^{23}Na nucleus.[48,49] Further, to facilitate direct voxel and slice-wise comparisons between these conventional measurements and ADC mapping, the latter's resolution can be increased using interleaved SPEN, and 3D volumetric coverage would be desirable to better characterize the full extent of the brain regions affected by stroke.[50,51] Therefore, technical improvements can continue to fill gaps in the ability to provide the highest sensitivity and specificity of each measurement of stroke individually to best optimize their performance when combined. By making these measurements at the cutting-edge field of 21.1 T, we have demonstrated the high performance of the individual measurements and established a set of longitudinal benchmarks that supports the potential of transitioning these and similar multiparametric approaches from lower-field to higher-field platforms to exploit their differential interparametric correlations and sensitivities to classify stroke and its recovery.

ACKNOWLEDGEMENTS

This work was performed at the US National High Magnetic Field Laboratory, which is supported by the National Science Foundation (CooperativeAgreements DMR-1157490 and DMR-1644779) and the State of Florida. Funding also was provided by the National Institutes of Health (R01 NS102395), an American Heart Association Grant-in-Aid (10DRNT3860040), the Minerva Foundation (Grant 712277) from the Federal German Ministry for Education and Research, the Kimmel Institute for Magnetic Resonance, the Perlman Family Foundation, the National Science Foundation International Research Fellowship Program, and the Fulbright Foundation.

ORCID

Avigdor Leftin https://orcid.org/0000-0002-4560-8162
Samuel C. Grant https://orcid.org/0000-0001-7738-168X
Lucio Frydman https://orcid.org/0000-0001-8208-3521

REFERENCES

1. Heit JJ, Zaharchuk G, Wintermark M. Advanced neuroimaging of acute ischemic stroke: Penumbra and Collateral Assessment. *Neuroimaging Clin N Am*. 2018;28:585-597.
2. Jauch EC, Saver JL, Adams HP, et al. Guidelines for the early management of patients with acute ischemic stroke: a guideline for healthcare professionals from the American Heart Association/American Stroke Association. *Stroke*. 2013;44:870-947.
3. Wey HY, Desai VR, Duong TQ. A review of current imaging methods used in stroke research. *Neurol Res*. 2013;35:1092-1102.
4. Albers GW, Thijs VN, Wechsler L, et al. Magnetic resonance imaging profiles predict clinical response to early reperfusion: the diffusion and perfusion imaging evaluation for understanding stroke evolution (DEFUSE) study. *Ann Neurol*. 2006;60:508-517.
5. Barber PA, Hoyte L, Kirk D, Foniok T, Buchan A, Tuor U. Early T1- and T2-weighted MRI signatures of transient and permanent middle cerebral artery occlusion in a murine stroke model studied at 9.4T. *Neurosci Lett*. 2005;388:54-59.
6. Chua JY, Pendharkar AV, Wang N, et al. Intra-arterial injection of neural stem cells using a microneedle technique does not cause microembolic strokes. *J Cereb Blood Flow Metab*. 2011;31:1263-1271.
7. Roberts TPL, Rowley HA. Diffusion weighted magnetic resonance imaging in stroke. *Eur Radiol*. 2003;45:185-194.
8. Wetterling F, Ansar S, Handwerker E. Sodium-23 magnetic resonance imaging during and after transient cerebral ischemia: multinuclear stroke protocols for double-tuned ^{23}Na/^{1}H resonator systems. *Phys Med Biol*. 2012;57:6929.
9. Bliss T, Guzman R, Daadi M, Steinberg GK. Cell transplantation therapy for stroke. *Stroke*. 2007;38:817-826.
10. Huang L, Liu Y, Lu J, Cerqueira B, Misra V, Duong TQ. Intraarterial transplantation of human ubilical cord blood mononuclear cells in hyperacture stroke improves vascular function. *Stem Cell Res Ther*. 2017;22:74.
11. Budinger TF, Bird MD, Frydman L, et al. Toward 20 T magnetic resonance for human brain studies: opportunities for discovery and neuroscience rationale. *Magn Reson Mater Phys Biol Med*. 2016;29:617-639.
12. Nagel AM, Umathum R, Rosler MB, et al. ^{39}K and ^{23}Na relaxation times and MRI of rat head at 21.1 T. *NMR Biomed*. 2016;29:759-766.
13. Schepkin VD, Brey WW, Gor'kov PL, Grant SC. Initial in vivo rodent sodium and proton MR imaging at 21.1 T. *Magn Reson Imaging*. 2010;28:400-407.
14. Hoult DI, Richards RE. The signal-to-noise ratio of the nuclear magnetic resonance experiment. *J Magn Reson*. 1976;24:71-85.
15. Markiewicz WD, Brey WW, Cross TA, et al. A decade of experience with the ultrawide-bore 900-MHz NMR magnet. *IEEE Trans Appl Supercond*. 2015;25:1501205.
16. Leftin A, Rosenberg JT, Solomon E, Calixto Bejarano F, Grant SC, Frydman L. Ultrafast in vivo diffusion imaging of stroke at 21.1 T by spatiotemporal encoding. *Magn Reson Med*. 2015;73:1483.
17. Rosenberg JT, Sellgren KL, Calixto-Bejarano F, et al. MR contrast and biological impacts of intracellular superparamagnetic iron oxides on human mesenchymal stem cells with hypoxic ischemic exposure. *Proc Int Soc Magn Reson Med*. 2012;8.

18. Rosenberg JT, Sellgren KL, Sachi-Kocher A, et al. Magnetic resonance contrast and biological effects of intracellular superparamagnetic iron oxides on human mesenchymal stem cells with long-term culture and hypoxic exposure. *Cytotherapy*. 2013;15:307-322.
19. Rosenberg J, Yuan X, Grant SC, Ma T. Tracking mesenchymal stem cells using magnetic resonance imaging. *Brain Circ*. 2016;2:108-113.
20. Maier O, Schröder C, Forkert ND, Martinetz T, Handels H. Classifiers for ischemic stroke lesion segmentation: a comparison study. *PLoS ONE*. 2015;10: e0145118.
21. Shen Q, Duong TQ. Quantiative prediction of ischemic stroke tissue fate. *NMR Biomed*. 2008;21:839-848.
22. Shen Q, Meng X, Fisher M, Sotak CH, Duong TQ. Pixel-by-pixel spatiotemporal progression of focal ischemia drived using quantiative perfusion and diffusion imaging. *J Cereb Blood Flow Metab*. 2003;23:1479-1488.
23. Wei L, Fraser JL, Lu ZY, Hu XY, Yu SP. Transplantation of hypoxia preconditioned bone marrow mesenchymal stem cells enhances angiogenesis and neurogenesis after cerebral ischemia in rats. *Neurobiol Dis*. 2012;46(3):635-645.
24. Fu R, Brey WW, Shetty K, et al. Ultra-wide bore 900 MHz high-resolution NMR at the National High Magnetic Field Laboratory. *J Magn Reson*. 2005;177:1-8.
25. Rosenberg JT, Shemesh N, Muniz JA, Dumez JN, Frydman L, Grant SC. Transverse relaxation of selectively excited metabolites in stroke at 21.1T. *Magn Reson Med*. 2017;77:520-528.
26. Ben-Eliezer N, Irani M, Frydman L. Super-resolved spatially encoded single-scan 2D MRI. *Magn Reson Med*. 2010;63:1594-1600.
27. Solomon E, Shemesh N, Frydman L. Diffusion weighted MRI by spatiotemporal encoding: analytical description and in vivo validations. *J Magn Reson*. 2013;232:76-86.
28. Campbell BC, Purushotham A, Christensen S, et al. The infarct core is well represented by the acute diffusion lesion: sustained reversal is infrequent. *J Cereb Blood Flow Metab*. 2012;32:50-56.
29. Wetterling F, Chatzikonstantinou E, Tritschler L, et al. Investigating potentially salvageable penumbra tissue in an in vivo model of transient ischemic stroke using sodium, diffusion, and perfusion magnetic resonance imaging. *BMC Neurosci*. 2016;17:82.
30. Wetterling F, Gallagher L, Mullin J, et al. Sodium-23 magnetic resonance imaging has potential for improving penumbra detection but not for estimating stroke onset time. *J Cereb Blood Flow Metab*. 2015;35:103-110.
31. Kraitchman DL, Bulte JW. Imaging of stem cells using MRI. *Basic Res Cardiol*. 2003;103:105-113.
32. Sumner JP, Shapiro EM, Maric D, Conroy R, Koretsky AP. In vivo labeling of adult neural progenitors for MRI with micron sized particles of iron oxide: quantification of labeled cell phenotype. *Neuroimage*. 2009;44:671-678.
33. Tarulli E, Chaudhuri JD, Gretka V, Hoyles A, Morshead CM, Stanisz GJ. Effectiveness of micron-sized superparamagnetic iron oxide particles as markers for detection of migration of bone marrow derived mesenchymal stromal cells in a stroke model. *J Magn Reson Imaging*. 2013;37:1409-1418.
34. Livne M, Kossen T, Madai VI, et al. Multiparametric model for penumbral flow prediction in acute stroke. *Stroke*. 2017;48:1849-1854.
35. Shen Q, Ren H, Fisher M, Bouley J, Duong TQ. Dynamic tracking of acute ischemic tissue fates using improved unsupervised ISODATA analysis of high-resolution quantitative perfusion and diffusion data. *J Cereb Blood Flow Metab*. 20045;24:887-897.
36. Sicard KM, Henninger N, Fisher M, Duong TQ, Ferris CF. Long-term changes of functional MRI-based brain function, behavioral status, and histopathology after transient focal cerebral ischemia in rats. *Stroke*. 2006;37:2593-2600.
37. Tsang A, Stobbe RW, Asdaghi N, et al. Relationships between sodium intensity and perfusion deficits in acute ischemic stroke. *J Magn Reson Imaging*. 2011;33:41-47.
38. Lin SP, Song SK, Miller JP, Ackerman JJ, Neil JJ. Direct, longitudinal comparison of ^{1}H and ^{23}Na MRI after transient focal cerebral ischemia. *Stroke*. 2001;32:925-932.
39. Kucharczyk J, Mintorovitch J, Asgari HS, Moseley M. Diffusion/perfusion MR imaging of acute cerebral ischemia. *Magn Reson Med*. 1991;19:50-67.
40. Thulborn KR, Gindin TS, Davis D, Erb P. Comprehensive MR imaging protocol for stroke management: tissue sodium concentration as a measure of tissue viability in nonhuman primate studies and in clinical studies. *Radiology*. 1999;213:156-166.
41. Artzi M, Aizenstein O, Jonas-Kimchi T, et al. Classification of lesion area in stroke patients during the subacute phase: a multiparametric MRI study. *Magn Reson Med*. 2014;72:1381-1388.
42. Kidwell CS, Wintermark M, De Silva DA, et al. Multiparametric MRI and CT models of infarct core and favorable penumbral imaging patterns in acute ischemic stroke. *Stroke*. 2013;44:73-79.
43. Li F, Liu KF, Silva MD, et al. Transient and permanent resolution of ischemic lesions on diffusion-weighted imaging after brief periods of focal ischemia in rats: correlation with histopathology. *Stroke*. 2000;31:946-954.
44. Nael K, Knitter JR, Jahan R, et al. Multiparametric magnetic resonance imaging for prediction of parenchymal hemorrhage in acute ischemic stroke after reperfusion therapy. *Stroke*. 2017;48:664-670.
45. Grant P, He J, Halpern E, et al. Frequency and clinical context of decreased apparent diffusion coefficient reversal in the human brain. *Radiology*. 2001;221:43-50.
46. Rosenberg JT, Sachi-Kocher A, Davidson MW, Grant SC. Intracellular SPIO labeling of microglia: high field considerations and limitations for MR microscopy. *Contrast Media Mol Imaging*. 2012;7:121-129.
47. Sart S, Bejarano FC, Baird MA, et al. Intracellular labeling of mouse embryonic stem cell-derived neural progenitor aggregates with micron-sized particles of iron oxide. *Cytotherapy*. 2015;17:98-111.
48. Konstandin S, Schad LR. 30 years of sodium/X-nuclei magnetic resonance imaging. *Magn Reson Mater Phys Biol Med*. 2014;27:1-4.

49. Riemer F, Solanky BS, Stehning C, Clemence M, Wheeler-Kingshott CA, Golay X. Sodium (^{23}Na) ultra-short echo time imaging in the human brain using a 3D-cones trajectory. *Magn Reson Mater Phys Biol Med*. 2014;27:35-46.

50. Schmidt R, Frydman L. New spatiotemporal appraoches for fully refocused, multisclice ultrafast 2D MRI. *Magn Reson Med*. 2014;71:711-722.

51. Liberman G, Frydman L. Reducing SAR requirments in multislice volumetric single-shot spatiotemporal MRI by two-dimensional RF pulses. *Magn Reson Med*. 2017;77:1959-1965.

How to cite this article: Leftin A, Rosenberg JT, Yuan X, Ma T, Grant SC, Frydman L. Multiparametric classification of sub-acute ischemic stroke recovery with ultrafast diffusion, ^{23}Na, and MPIO-labeled stem cell MRI at 21.1 T. *NMR in Biomedicine*. 2019;e4186. https://doi.org/10.1002/nbm.4186